AIMS Mathematics, 10(8): 18801–18823.
DOI: 10.3934/math.2025840
Received: 09 April 2025
Revised: 01 July 2025
Accepted: 15 July 2025
Published: 19 August 2025

https://www.aimspress.com/journal/Math

Research article

Dynamic evolution sequence set-assisted machine tool interval analysis

Xindi Wei[1,†], Jin Deng[2,†,*], Shizhong Liang[1] and Yu Ye[2]

[1] State Key Laboratory of Structural Analysis, Optimization and CAE Software for Industrial Equipment, School of Mechanics and Aerospace Engineering, Dalian University of Technology, Dalian 116024, China

[2] Yunnan Branch of China Academy of Machinery Co., Ltd., Yunnan Provincial Key Laboratory of Mechatronics Application Technology, 309 Hongling Road, Wuhua District, Kunming City, Yunnan, China

[†] These authors contributed equally to this work and are co-first authors

[*] **Correspondence:** Email: dengjin1989km@163.com.

Abstract: This paper investigates the uncertainty of machine tools and proposes an efficient interval uncertainty analysis framework for machine tools. This problem involves interval analysis and the calculation of machine tool response. The traditional analysis method has drawbacks, including low computational efficiency and the need to collect a large amount of sample information. In this paper, the intelligent optimization algorithm is used to analyze the interval of the machine tool, and the interval analysis results can be obtained by using less sample information, which improves the efficiency of the interval analysis. The dynamic evolution sequence (DES) is used to optimize the search sequence of the artificial bee colony (ABC) algorithm to improve the computational efficiency and accuracy of the optimization algorithm. To address the problem of the high computational cost of the finite element model, the Kriging surrogate model is used to replace complex finite element calculations. To achieve better calculation accuracy, this paper utilizes the DES to optimize the Kriging model, resulting in a significant improvement in the calculation accuracy of the improved Kriging model (DES-Kriging). Combining DES-ABC and DES-Kriging, this paper proposes a new interval uncertainty analysis framework and verifies the accuracy and efficiency of this interval analysis framework by numerical experiments.

Keywords: uncertainty analysis; intelligent optimization algorithm; dynamic evolution sequence; Kriging surrogate model; machine tool stability
Mathematics Subject Classification: 65C05, 74P10, 90C29

Abbreviations: DES: dynamic evolution sequence; ABC: artificial bee colony; DES-Kriging: the improved Kriging model; DES-ABC: the improved artificial bee colony

1. Introduction

The gantry machine tool, a large-scale computer numerical control system, is specifically designed for machining large, heavy, and complex workpieces. Characterized by high precision, efficiency, and automation capabilities, this equipment has become indispensable in modern manufacturing [1–3]. Its innovative structural configuration incorporates a stationary worktable and a dynamically driven crossbeam. During operation, the beam, as the main moving part, must simultaneously bear its inertial load and the gravity of key subsystems, such as sliding saddles, and maintain good performance to ensure fast and smooth processing performance [4]. Conventional crossbeam assembly typically employs bolted connections, a method preferred for its maintenance accessibility and component modularity. However, this approach inherently creates extended interfacial contact zones between structural members, introducing localized stiffness discontinuities within the machine tool's framework [5]. Empirical studies reveal that 60%–80% of a machine tool's stiffness originates from these interconnected component interfaces [6]. Consequently, the stiffness characteristics of the crossbeam joint play an extremely crucial role in the performance of the machine tool.

Uncertainty is a common issue in practical engineering [7–10] and is essential for providing more comprehensive risk assessment and decision-making support for complex engineering problems [11,12]. The specific conditions of the machine tool crossbeam joint are highly complex and may be influenced by various factors such as pre-tightening force [13], surface roughness [14], and material properties [15], leading to significant uncertainty in the performance of the joint. During the operation of the machine tool, the stiffness and deformation of the machine tool joint can affect the machining accuracy and the stability of the machine tool [16]. Since the stiffness of the machine tool mainly originates from the joints, it is crucial to conduct an uncertainty analysis on the stiffness of these joints. If a large number of uncertainty samples corresponding to different stiffness levels and machine tool responses could be measured, the responses could be described using stochastic models based on probability theory [18]. However, in practice, it is often difficult to measure the exact stiffness of the machine tool joints and to obtain the corresponding machine tool responses for different stiffness levels. For such uncertainty variables with insufficient sample size and missing sample information, namely epistemic uncertainty variables, interval models are commonly employed for description, and interval uncertainty analysis is conducted. Interval uncertainty analysis is typically regarded as an extremum problem, which can be solved using optimization algorithms. Among them, intelligent optimization algorithms are frequently used in various optimization problems due to their diversity and flexibility [17,18].

Among intelligent optimization algorithms, the artificial bee colony (ABC) algorithm [19] has the advantages of fewer parameters, high computational efficiency, and strong global search capabilities, making it an effective tool for solving complex optimization problems. It has been successfully applied in areas such as engineering optimization [20], energy conservation and emission reduction [21], and path planning [22]. Applying the ABC algorithm in the uncertainty analysis of machine tool stiffness can more quickly and accurately identify the response bounds. However, the ABC algorithm, which searches for optimization through the generation of random sequences, has the

disadvantage of being unable to effectively cover the search space because of the non-uniform distribution of the sequences. Wu et al. [23] demonstrated that replacing the random variables in intelligent evolutionary algorithms with low-discrepancy sequences (LDS), which have better uniformity, can effectively generate offspring samples to cover the solution space, thereby significantly improving computational efficiency. Common LDS include the Halton sequence [24] and the dynamical evolution sequence (DES) [25]. Among the tested LDS, DES has the most significant improvement effect [23]. Therefore, we adopted the more uniform DES point set to optimize the ABC algorithm, thereby further enhancing the global search capability of ABC. The DES-ABC algorithm can quickly and precisely identify the interval range of key point responses, assisting us in conducting an interval uncertainty analysis of the machine tool.

Although the DES-ABC algorithm can help us quickly identify the interval range of key point responses, using finite element models [26,27] for analysis in interval analysis still consumes a significant amount of time. During the solution process of finite element analysis, due to the large size and complex structure of the machine tool, the corresponding high-precision finite element model often contains a large number of nodes, which significantly increases the computation time for each finite element analysis. When conducting an uncertainty analysis of the machine tool's finite element model, multiple repeated solutions are usually required, which greatly reduces the efficiency of model analysis. To address this issue, current researchers typically employ the method of constructing surrogate models to simplify the calculations [28–30]. Among many surrogate models, the Kriging model captures the spatial correlation of data to provide high-precision predictions and quantify error estimates. It has the advantages of strong adaptability, good continuity of prediction results, and outstanding optimization capabilities, making it particularly suitable for the modeling and optimization of complex systems [31,32]. Under normal circumstances, the accuracy of the Kriging model is proportional to the number of training sample points. However, due to the limitations of simulation computational costs, we hope to construct a high-precision surrogate model using as few sample points as possible. Studies have shown that the uniformity of the sample point set is closely related to the accuracy of the Kriging model. The more uniformly the sample points are distributed, the higher the accuracy of the generated Kriging model [33]. By introducing a more uniform DES sequence to replace the initial sample set in the Kriging model, the accuracy of the Kriging model can be improved, thereby more accurately identifying the responses at different locations of the machine tool.

Based on the DES-ABC algorithm and DES-Kriging model, this paper proposes a new framework for interval uncertainty analysis of machine tools, which can efficiently and accurately analyze the interval of machine tools. The remaining structure of this paper is as follows: Section 2 briefly introduces the interval uncertainty analysis method and the ABC algorithm; Section 3 introduces the improved ABC algorithm and the Kriging model and presents the framework for interval analysis in this paper; Section 4 verifies the effectiveness of the proposed method through three numerical examples; Section 5 concludes and provides an outlook.

2. Uncertainty analysis

2.1. Interval uncertainty analysis

In engineering practice, numerous scenarios involve insufficient probabilistic distribution information, where interval modeling serves as an effective approach for characterizing uncertainty

variables [34]. Interval uncertainty analysis represents uncertain parameters through bounded intervals rather than single-point estimates or probability distributions [35,36], thereby establishing a more robust and conservative framework for uncertainty modeling. When employing interval models for uncertainty representation, the uncertain variable $\boldsymbol{x}$ is defined as an interval variable, mathematically expressed as:

$$\boldsymbol{x} = \left[x_1, x_2, \cdots, x_D\right], x_{i,\min} \le x_i \le x_{i,\max}, \tag{2.1}$$

where D represents the dimension of the interval variable, $x_{i,\min}$ and $x_{i,\max}$ represent the lower and upper bounds of the i-th element, respectively. The general interval analysis model is formulated as:

$$\boldsymbol{y} = f\left(\boldsymbol{x}\right), \tag{2.2}$$

where represents the response function, and $\boldsymbol{y}$ corresponds to the system response. When inputs exist as interval variables, the response becomes a bounded range rather than a deterministic value. If the number of responses is n, the response $\boldsymbol{y}$ can be expressed as: $\boldsymbol{y} = \left[y_1, y_2, \cdots, y_n\right], y_i \in \left[y_{i,\min}, y_{i,\max}\right]$ The critical task in interval uncertainty analysis involves determining the extremal bounds of target responses, which effectively transforms the problem into $2n$ optimization subproblems: one for maximizing and another for minimizing each response component. This dual optimization framework provides quantifiable boundaries for structural uncertainty analysis:

$$\begin{cases} \min\ y_i, \\ \max\ y_i, \end{cases} i = 1, 2, \cdots, M, \tag{2.3}$$

By performing interval uncertainty analysis on the uncertain variable $\boldsymbol{x}$, we can determine the minimum and maximum values of its response, denoted as $\boldsymbol{y}_{\min}$ and $\boldsymbol{y}_{\max}$, respectively, thereby identifying the bounds of the output response.

In the interval analysis of the machine tool beam in this paper, we consider the combined stiffness $\boldsymbol{K} = \left[K_1, K_{2,} \cdots K_8\right]$ and the applied force position r as uncertain variables. Taking the range of uncertain variables $\left[\boldsymbol{K}_{\min}, \boldsymbol{K}_{\max}\right]$ and $\left[r_{\min}, r_{\max}\right]$ as input, the displacement response range of the key parts of the machine tool beam $\left[\boldsymbol{w}_{\min}, \boldsymbol{w}_{\max}\right]$ is obtained by interval analysis. Determining these response bounds provides essential insights for structural optimization design and machining accuracy enhancement, ensuring that beam deformation remains within acceptable limits under varying operational conditions, thereby guaranteeing overall machine performance and stability.

2.2. The ABC algorithm

The ABC algorithm [19] is a swarm intelligence optimization technique inspired by honeybee foraging behavior, renowned for its strong global search capability and rapid convergence. By simulating the social structure and cooperative mechanisms of bee colonies, ABC effectively addresses optimization problems through three distinct bee roles: employed bees, onlooker bees, and scout bees. The collective objective is to locate the nectar-rich food source corresponding to the minimum fitness value in the solution space. For a D-dimensional optimization problem with N employed bees and

$\frac{N}{2}$ onlooker bees, let the objective function be $f(\cdot)$. Each candidate solution is represented as $\boldsymbol{x}=(x_1,x_2,\cdots,x_D)^{\mathrm{T}}\in\mathbb{R}^{D\times 1}$, where $\mathbb{R}$ is a real number set, with corresponding fitness $\boldsymbol{y}=f(\boldsymbol{x})$. The ABC workflow comprises:

(1) Initialization phase:

Randomly generate N initial food sources via:

$$\boldsymbol{x}_i=\boldsymbol{x}_{\min}+\boldsymbol{\varphi}_i^{\mathrm{ini}}\circ(\boldsymbol{x}_{\max}-\boldsymbol{x}_{\min}),\ i=1,2,\cdots,N, \tag{2.4}$$

where $\boldsymbol{x}_i$ represents the specific position of the i-th food source, $\boldsymbol{x}_{\max}$ and $\boldsymbol{x}_{\min}$ denote the upper and lower bounds of each uncertain element in the food source, and $\boldsymbol{\varphi}^{\mathrm{ini}}\in\mathbb{R}^{D\times N}$ is a random matrix with elements uniformly distributed in the range [0, 1], and the elements are mutually independent. The i-th row of the matrix $\boldsymbol{\varphi}^{\mathrm{ini}}$ is denoted as $\boldsymbol{\varphi}_i^{\mathrm{ini}}$.

(2) Employed bee phase:

For each food source $\boldsymbol{x}_i$, the employed bees search within their neighborhood according to the following formula to generate a new food source $\boldsymbol{v}_i$:

$$\boldsymbol{v}_i=\boldsymbol{x}_i+(2\boldsymbol{\varphi}_i^{\mathrm{emp}}-1)\circ(\boldsymbol{x}_i-\boldsymbol{x}_k),\ i=1,2,\cdots,N, \tag{2.5}$$

where k is a randomly selected food source different from i, and $\boldsymbol{\varphi}^{\mathrm{emp}}\in\mathbb{R}^{D\times N}$ is a random matrix whose elements are all in the range [0, 1], and the elements are mutually independent. Then calculate the fitness value $f(\boldsymbol{v}_i)$ and compare it with the fitness value $f(\boldsymbol{x}_i)$, and retain the food source with a better-fitness value.

(3) Onlooker bee phase:

Onlooker bees set the roulette parameters according to the magnitude of the fitness function $f(\boldsymbol{x}_i)$ in proportion. They select the food source x_p according to the roulette-wheel selection strategy, as detailed in literature [32]. After the onlooker bees select the food source, a new candidate food source position $\boldsymbol{v}_i^*$ is generated near the food source x_p in the following way:

$$\boldsymbol{v}_i^*=\boldsymbol{x}_i+(2\varphi_i^{\mathrm{onl}}-1)\circ(\boldsymbol{x}_i-\boldsymbol{x}_p), \tag{2.6}$$

where $\boldsymbol{\varphi}^{\mathrm{onl}}\in\mathbb{R}^{D\times\frac{N}{2}}$ is a random matrix whose elements are all in the range [0, 1], and the elements are mutually independent. $\boldsymbol{x}_i$ is a randomly selected food source different from $\boldsymbol{x}_p$. Calculate the fitness values of the new food sources selected by $\frac{N}{2}$ onlooker bees. Similarly, compare the fitness of the original food source and the new food source, and retain the food source with higher fitness.

(4) Scout bee phase:

If a certain food source has not been updated in R consecutive iterations, it is considered that

the solution at this place has fallen into a local optimum, and this food source is abandoned. If the food source is abandoned, the corresponding bee transforms into a scout bee. The scout bee randomly generates a new food source position:

$$\boldsymbol{x}_i^{\text{new}} = \boldsymbol{x}_{\min} + \left(2\boldsymbol{\varphi}_i^{\text{sco}} - 1\right) \circ \left(\boldsymbol{x}_{\max} - \boldsymbol{x}_{\min}\right), i = 1, 2 \cdots M, \tag{2.7}$$

where $\boldsymbol{\varphi}^{\text{sco}} \in \mathbb{R}^{D \times M}$ is a random matrix whose elements are all in the range [0, 1], where M is the number of food sources that need to be re-initialized during this iteration process.

(5) Repeat phases (1)–(4) until termination, recording the position and fitness value of the best food source per generation.

While ABC effectively balances global and local search capability through swarm intelligence, its reliance on random initialization and stochastic search vectors introduces spatial distribution inhomogeneity, potentially compromising search efficiency and solution quality. To address this, we propose the DES-ABC algorithm by integrating DES to optimize ABC's initialization and search mechanisms.

3. Efficient machine tool interval analysis framework, DAK

In the interval analysis of machine tools, an efficient and accurate interval modeling framework for machine tools in combination with the DES-ABC algorithm is proposed. Compared with the traditional Monte Carlo method, which is characterized by a large sample size and low computational efficiency, the proposed method in this paper can significantly enhance the efficiency and accuracy of interval analysis. To address the large number of finite element model nodes and time-consuming analysis, a DES-Kriging model of the machine tool crossbeam was established in this paper to replace the finite element model, thereby improving the computational efficiency of the machine tool response.

3.1. Improved Kriging surrogate model based on DES (DES-Kriging)

In the context of machine tool structure optimization, model updating often encounters the issue of high computational complexity associated with finite element analysis. To address this challenge, surrogate models are commonly employed to achieve efficient computation. Kriging model is an interpolation method based on spatial autocorrelation. It has been widely used to predict unknown points by optimal unbiased estimation. The construction process of the Kriging model can be referred to in literature [38]. The first step in building a Kriging model is to obtain a suitable sample set for model construction by inputting the finite element model to get the corresponding results. Traditional Kriging modeling typically employs Latin Hypercube Sampling (LHS) [39] to construct the initial sample set. However, this approach has limitations in terms of spatial uniformity. Uniform sampling strategies can improve the uniformity of the sampling space, better capture the spatial characteristics of the finite element model, reduce interpolation errors, and enhance the accuracy of the surrogate model. In this paper, we introduce the DES point set, which exhibits stronger uniformity in high-dimensional spaces.

The static solutions of multi-body systems often exhibit good uniformity. Inspired by this, Wu et al. [25] proposed DES. Assume that all samples are within the D-dimensional unit cube, and each sample is regarded as a star with a mass of m. The coordinate of the i-th star is $\boldsymbol{x}_i = \left(x_{i1}, \cdots, x_{iD}\right)$,

and there are interaction forces between points. The Lagrangian equations of the stars are expressed as:

$$\begin{cases} S = \int_0^t L \mathrm{d}\tau \\ L = \frac{1}{2} m \sum_{i=1}^{N} \sum_{k=1}^{D} \dot{x}_{ik}^2 - G\left(\sum_{1 \le i < j \le N} \frac{1}{d_{q,ij}^p} \right)^{\frac{1}{p}} \end{cases}, \tag{3.1}$$

where $G = 1$ represents the generalized gravitational constant; q and p are control parameters; and $d_{q,ij}$ is the generalized distance. The values can be found in the literature [25]. According to Hamilton's variational principle [27,40], it can be obtained that,

$$m\ddot{x}_{ik} + c\dot{x}_{ik} + f_{ik} = 0,\ 1 \le i \le N,\ 1 \le k \le D, \tag{3.2}$$

where c is an artificial damping coefficient. When the system is static, the sequence $\boldsymbol{X}_{D,N} = \{\boldsymbol{x}_1, \boldsymbol{x}_2, \cdots, \boldsymbol{x}_N\}$ composed of the obtained galaxy coordinates $\boldsymbol{x}_i$ can be regarded as LDS.

Given that DES maintains good uniformity in high-dimensional spaces, this study employs DES as the initial sampling set for the Kriging model, which is then input into the finite element model. This approach yields results that more accurately reflect the spatial characteristics of the finite element model, thereby effectively enhancing the model's predictive accuracy [41]. In Section 4.2, we will use a numerical example to prove that using the DES-Kriging model to construct the machine tool surrogate model can more accurately calculate the response of the machine tool.

3.2. Improved ABC based on DES (DES-ABC)

Wu et al. [23] demonstrated that, in intelligent evolutionary algorithms, replacing random variables with low-discrepancy sequences with better uniformity can effectively generate offspring samples that cover the solution space, thus significantly improving computational efficiency. Among the tested low-discrepancy sequences, DES has the most remarkable improvement effect. Therefore, we choose the DES point set to improve the ABC algorithm.

Assume that a DES of size $D \times N$, called $\boldsymbol{P}$, is obtained by Eqs (2.4)–(2.7).

$$\boldsymbol{P} = \begin{bmatrix} p_{11} & p_{12} & \cdots & p_{1N} \\ p_{21} & p_{22} & \cdots & p_{2N} \\ \vdots & \vdots & \ddots & \vdots \\ p_{D1} & p_{D2} & \cdots & p_{DN} \end{bmatrix} = \begin{bmatrix} \boldsymbol{p}_{1,:} \\ \boldsymbol{p}_{2:} \\ \vdots \\ \boldsymbol{p}_{D,:} \end{bmatrix}. \tag{3.3}$$

So, each column vector of $\boldsymbol{P}$ can be used to replace the random vector $\boldsymbol{\varphi}_i$ in Eqs (2.4)–(2.7), making the offspring cover the solution space more uniformly. However, it causes ABC to lose the randomness [42]. In order to make the ABC enhance uniformity while preserving randomness, a method called dimension random rearrangement (DRR) is proposed. The specific steps of DRR are as follows:

A. Let $I_0 := \{1, 2, ..., D\}$ and randomly select a number $\Phi_{1,1}$ from I_0, random selection is

performed by drawing without replacement from the remaining set of dimensions;

B. Let $j = 1, 2, ..., D$ and do the following loop,

a) Put the $\Phi_{1,j}$-th row elements in $\boldsymbol{P}$ into the j-th row elements of $\boldsymbol{P}_{\boldsymbol{\Phi}}$;

b) $I_j = I_{j-1} - \Phi_{1,j}$. This operation denotes, removing the selected number $\Phi_{1,j}$ from the set I_{j-1} to generate the new set I_j;

c) Randomly select a number $\Phi_{1,j}$ from the set I_j.

Finally, a new sequence $\boldsymbol{P}_{\boldsymbol{\Phi}}$ with randomness is generated by the above operations,

$$\boldsymbol{P}_{\boldsymbol{\Phi}_1} = \begin{bmatrix} p_{\phi_{1,1},1} & p_{\phi_{1,1},2} & \cdots & p_{\phi_{1,1},N} \\ p_{\phi_{1,2},1} & p_{\phi_{1,2},2} & \cdots & p_{\phi_{1,2},N} \\ \vdots & \vdots & \ddots & \vdots \\ p_{\phi_{1,D},1} & p_{\phi_{1,D},2} & \cdots & p_{\phi_{1,D},N} \end{bmatrix} = \begin{bmatrix} \boldsymbol{p}_{\phi_{1,1},:} \\ \boldsymbol{p}_{\phi_{1,2},:} \\ \vdots \\ \boldsymbol{p}_{\phi_{1,D},:} \end{bmatrix}. \tag{3.4}$$

Based on the above content, the construction process is as follows: continuously select row indices randomly from the initial set of row numbers, fill the new matrix with the corresponding rows from the original matrix, and update the set to avoid repetition. This ultimately allows the matrix rows to be rearranged in a random and non-repetitive order for the matrix $\boldsymbol{P}_{\Phi}$.

It can be proved that the uniformity of $\boldsymbol{P}_{\Phi}$ is the same as that of $\boldsymbol{P}$. There are many commonly used discrepancies to measure uniformity, such as L_2 discrepancy, MD discrepancy, and WD discrepancy [43]. Taking L_2 discrepancy as an example, its calculation formula is as follows:

$$D_{L_2}(\boldsymbol{P})^2 = \left(\frac{1}{3}\right)^D - \frac{2}{D}\sum_{j=1}^{N}\prod_{i=1}^{D}\left(\frac{1-p_{ij}^2}{2}\right) + \frac{1}{D^2}\sum_{j,l=1}^{N}\prod_{i=1}^{D}\left[1-\max\left(p_{ij}, p_{il}\right)\right]. \tag{3.5}$$

Replacing $\boldsymbol{P}$ in Eq (3.5) with $\boldsymbol{P}_{\boldsymbol{\Phi}}$ from Eq (3.4), it can be obtained that the L_2 discrepancy of $\boldsymbol{P}_{\boldsymbol{\Phi}}$ is

$$D_{L_2}\left(\boldsymbol{P}_{\boldsymbol{\Phi}_g}\right)^2 = \left(\frac{1}{3}\right)^D - \frac{2}{D}\sum_{j=1}^{N}\prod_{i=1}^{D}\left(\frac{1-p_{\phi_{g,i},j}^2}{2}\right) + \frac{1}{D^2}\sum_{j,l=1}^{N}\prod_{i=1}^{D}\left[1-\max\left(p_{\phi_{g,i},j}, p_{\phi_{g,i},l}\right)\right]. \tag{3.6}$$

It can be derived that,

$$D_{L_2}(\boldsymbol{P})^2 = D_{L_2}\left(\boldsymbol{P}_{\boldsymbol{\Phi}_g}\right)^2. \tag{3.7}$$

From this, it can be seen that the DRR method only changes the order of matrix rows in high-dimensional space, while the cumulative product of the same column of the matrix remains unchanged. This means that DRR does not change the numerical values and distribution of the data itself, but only adjusts the arrangement of the data. The relative differences between samples and the statistical characteristics of the overall data have not changed. Random techniques such as perturbation and jittering will directly change the values of sample data or their distribution characteristics [44], causing the uniformity of samples to change.

If G random matrices are needed in the iterative process of ABC algorithm, DRR the DES $\boldsymbol{P}$ $G-1$ times to generate $G-1$ different LDSs of $D\times N$ size, named $\boldsymbol{P}_{\Phi_1}, \boldsymbol{P}_{\Phi_2}, \ldots, \boldsymbol{P}_{\Phi_{G-1}}$. Each column vector of $\boldsymbol{P}$ and $\boldsymbol{P}_{\Phi_g}$ can be used to replace the random vector φ_i in Eqs (2.4)–(2.7), making the offspring cover the solution space more uniformly to enhance the efficiency. The more efficient ABC based on DES is called DES-ABC.

3.3. An efficient and accurate framework for interval analysis of machine tools

When conducting interval analysis of machine tools, the following issues arise: 1) The traditional Monte Carlo method requires a large number of samples to identify the response boundaries, resulting in low computational efficiency. 2) The finite element model comprises a vast number of nodes, and finite element analysis consumes a significant amount of time. In view of the above two problems, we use the DES-Kriging model to establish the finite element model of the beam, and use the DES-ABC algorithm to analyze the interval of the machine tool. The DES-Kriging machine tool agent can quickly and accurately obtain the response range of the dangerous position and improve the computational efficiency of the machine tool response. DES-ABC algorithm can quickly find the interval range of machine tool response because of its strong global search ability. We name this interval analysis method combining DES-ABC algorithm and DES-Kriging model as DAK, and the calculation framework is shown in Figure 1.

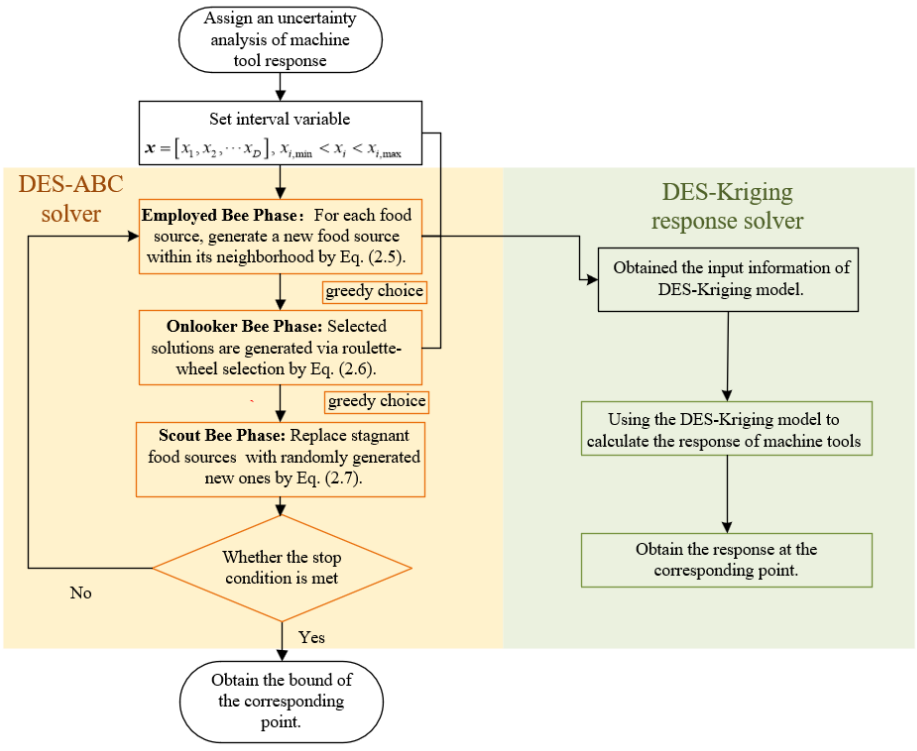

Figure 1. The framework of the interval analysis method for machine tools (the termination conditions for the DES-ABC algorithm are: reaching a certain number of iterations or no improvement between consecutive iterations).

The yellow section in the figure represents the solution process of the DES-ABC solver, while the green section illustrates the calculation of the responses at corresponding points using the DES-Kriging model of the machine tool. According to the literature [45], we adopted the maximum number of iterations as one of the termination conditions for the algorithm; the other termination condition is that when the change in the objective function value over consecutive iterations of the algorithm is less than a set threshold, the algorithm is considered to have converged, and the iterations can be stopped. At this point, combined with the DES-ABC algorithm and the DES-Kriging model, this paper proposes an efficient and accurate machine tool interval analysis framework, DAK. The DAK can effectively evaluate the impact of uncertainties in the connection of the machine tool's crossbeam on the stability of the machine tool. In Section 4 of this paper, three numerical examples are given to verify the accuracy and efficiency of the DAK.

The DAK method proposed by us demonstrates broad applicability in practical problems, especially suitable for complex engineering issues that involve high-dimensional parameter spaces, high computational costs, and require efficient uncertainty analysis. This includes performance assessment challenges due to parameter uncertainty (such as connection stiffness, load positions, etc.) in other machine tool components, manufacturing equipment, aerospace and other engineering systems. It provides an efficient and reliable analytical tool for design optimization and stability assurance.

4. Numerical experiments

4.1. Performance comparison between ABC and DES-ABC algorithm

To evaluate the optimization performance of the DES-ABC algorithm, this study selected five benchmark test functions [46] to validate the algorithm's performance. The Table 1 provides detailed information on the naming conventions, mathematical characteristics, and global optimal solutions of each test function（F_i^*）.

Table 1. Detailed information of benchmark test functions.

Fn	Functions	F_i^*
F1	Shifted and full rotated expanded Schaffer's f6 function	600
F2	Shifted and full rotated Levy function	900
F3	Hybrid function 1	2000
F4	Hybrid function 2	2200
F5	Composition function	2300

The specific forms of F1–F5 are shown in the appendix.

To ensure fairness in the experimental design, the core control parameters of the comparison algorithms are uniformly configured, with the population size set to 40. The limit value is a specific control parameter of the ABC algorithm, which is determined by the following formula:

$$h = \frac{N}{2} \times D, \tag{4.1}$$

where N represents the population size of the swarm, and D denotes the dimensionality of the optimization problem. In this experiment, $D = 10, 20$. The maximum number of iterations G is used as the termination condition of the experiment, with values of 2000 and 4000 for $D = 10$ and $D = 20$, respectively. The parameters were determined based on literature [47] and validated through preliminary experiments to balance computational efficiency and accuracy. The algorithm parameters are shown in Table 2.

Table 2. Algorithm parameter settings.

D	N	G	$h = N/2 \times D$
$D = 10$	40	2000	200
$D = 20$	40	4000	400

According to literature [46], the computational complexities O of the DES-ABC algorithm and the ABC algorithm can be calculated, and the results are shown in Table 3.

Table 3. Comparison of computational complexity between DES-ABC and ABC.

	The computational complexity of an algorithm			
No.	T_0	T_1	T_2	O
DES-ABC	0.0060	0.3106	1.3074	166.1
ABC		0.3296	1.2950	160.9

As shown in Table 3, the computational complexities of the DES-ABC algorithm and the ABC algorithm are not significantly different, which indicates that the calculation times of DES-ABC and ABC algorithms are basically the same under the same maximum number of iterations. Therefore, improving the ABC algorithm with the DES sequence does not affect the iteration speed of the algorithm.

To minimize the interference of randomness in the optimization process on the results, we execute each algorithm 30 times. Based on this, the optimization performance of the two algorithms is comprehensively evaluated by the mean convergence value of the objective function and the number of iterations required for the objective function error ε_{tol} to converge to 5%. We also performed a Wilcoxon rank-sum test on the computational results of the ABC algorithm and the DES-ABC algorithm to determine if there is a statistically significant difference in the performance of the two algorithms using a significance level.

In Table 4, p_{mean} represents the significance level of the mean value, and $p_{\text{i-s}}$ represents the significance level of the number of iterations. The comparison of the performance of the algorithm is as follows. We coarsen the data that represents better performance.

Table 4. The results of 30 independent runs of the numerical function of the ABC algorithm.

Func		ABC		DES-ABC		Wilcoxon rank-sum test	
	D	Mean	$\varepsilon_{tol}=5\%$ iteration step	Mean	$\varepsilon_{tol}=5\%$ iteration step	p_{mean}	$p_{\text{i-s}}$
F_1	10	600.0204	44	600.0002	25	3.02×10^{-11}	1.68×10^{-10}
	20	600.1367	109	600.0000	60	3.02×10^{-11}	2.95×10^{-11}
F_2	10	902.2219	167	900.0000	68	3.02×10^{-11}	1.92×10^{-9}
	20	955.0710	3369	900.0000	791	3.02×10^{-11}	1.20×10^{-10}
F_3	10	2058.5263	89	2045.9783	20	1.87×10^{-5}	1.01×10^{-2}
	20	2054.7834	205	2045.8405	120	3.47×10^{-10}	2.47×10^{-7}
F_4	10	2229.9749	8	2225.6350	1	4.64×10^{-3}	4.42×10^{-9}
	20	2228.0192	20	2226.0817	16	2.23×10^{-9}	1.59×10^{-5}
F_5	10	2401.5439	1203	2400.0217	467	3.02×10^{-11}	2.92×10^{-11}
	20	2406.3306	3536	2400.0009	926	3.02×10^{-11}	3.01×10^{-11}

As can be seen from the table above, the average optimal objective function values obtained by the DES-ABC algorithm are lower than those by the ABC algorithm across different dimensions. The average error of the ABC algorithm is calculated to be 2.37%, while that of the DES-ABC algorithm is 1.56%. This indicates that the computational accuracy of the DES-ABC algorithm is enhanced by 80% compared with the ABC algorithm. The number of iterations required for the traditional ABC algorithm to achieve an average error convergence within 5% is more than 3.5 times that of the DES-ABC algorithm, which implies that the computational efficiency of the DES-ABC algorithm is improved by a factor of 3.5 compared with the traditional ABC algorithm. The results obtained from the Wilcoxon rank-sum test are all less than the significance level p=0.05, indicating that there is a statistically significant difference in the performance of these two algorithms. These results demonstrate that the DES-ABC algorithm possesses higher computational accuracy and efficiency.

4.2. Accuracy verification of DES-Kriging model of the machine tool beam

The research object of this case is a machine tool crossbeam model. Due to the strong uncertainty of the machine tool joint and the fact that the stiffness of the joint in the machine tool accounts for approximately 60%–80% of the total stiffness of the machine tool [6], the stiffness of the machine tool joint is selected as an uncertain variable, and the uncertain analysis of the machine tool is carried out in combination with the force-bearing position of the slider on the guide rail. The geometric midpoint of the crossbeam is used as the coordinate origin to establish a three-dimensional XYZ coordinate system. The material of the crossbeam has an elastic modulus of $E_0 = 2\times10^{11}$ Pa and a Poisson's ratio of $\mu = 0.3$. The bottom of the machine tool crossbeam is fastened to the column via bolts, resulting in a semi-rigid connection structure. Due to the structural discontinuity introduced by bolted connections in machine tool assembly, it is necessary to focus on the performance evaluation of the connection area. In this study, to simulate the joint's connection characteristics, eight Y-directional spring elements were incorporated at the crossbeam-column interface surfaces. Additionally, to achieve accurate representation of the crossbeam's structural performance, movement in the X and Z

directions was restricted in the finite element analysis. The specific locations of the applied spring elements are illustrated in Figure 2(a).

The machine tool structure was discretized using finite element analysis, yielding a computational mesh comprising 376,547 nodes and 195,475 elements. The model considers the self-weight of the crossbeam and external forces from other components. These forces are simulated as a remote force with a magnitude of 25,454 N and a direction along the negative Y-axis; the specific situation can be referred to Figure 2(b).

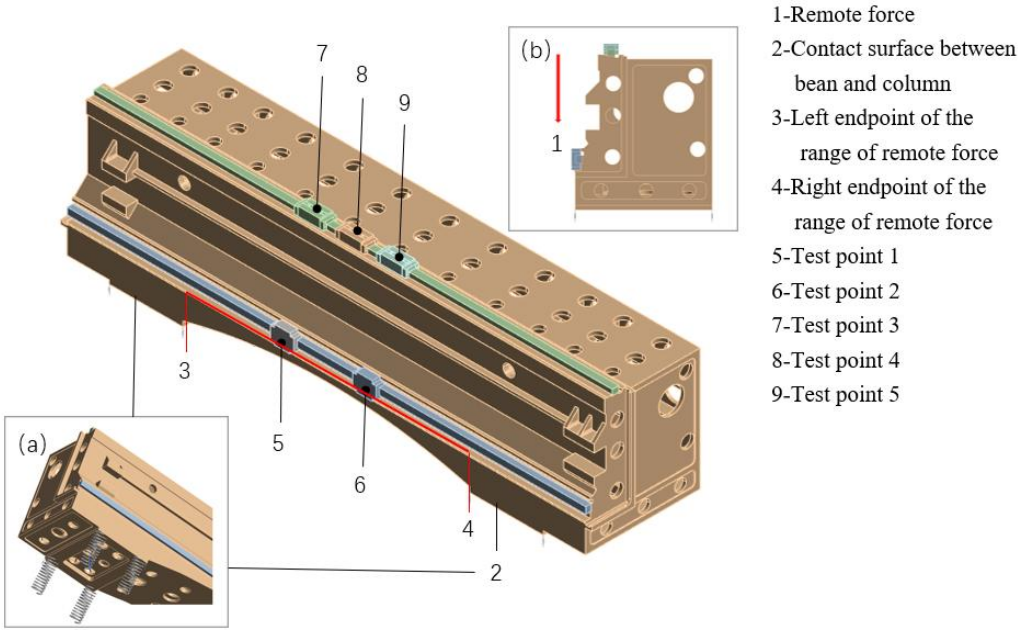

Figure 2. Beam model of gantry machine tool.

In this study, the force can move along the Y-axis, and the application position of the force along the Z-axis, as well as the stiffness coefficients of the eight spring elements, are treated as input variables. The specific information on these variables is listed in Table 5.

Table 5. Remote force position and spring element stiffness information.

Unknown variable	Distribution range
Position of the applied force	[-1,1] m
Stiffness of 8 spring elements	$[3\times10^{9},1\times10^{10}]$ N/m

As depicted in Figure 2, the midpoints of five slide pillow planes are selected as measurement points. The DES sequence of dimension 9 is selected as the sample point set, composed of 100 uniformly distributed sample points. These sample points are utilized as input parameters for the finite element analysis of the machine tool, and the deformation responses of the five measurement points are computed as the output results. Subsequently, a DES-Kriging model for the machine tool is developed. The DES-Kriging model is applied to compute a random sample, and the results are presented in Table 6.

Table 6. The measured data compared with the predicted results.

	Response result (m)					Calculation time (s)
No.	1	2	3	4	5	
finite element model	3.12×10^{-5}	2.99×10^{-5}	3.13×10^{-5}	3.22×10^{-5}	3.06×10^{-5}	46
DES-Kriging model	3.05×10^{-5}	3.05×10^{-5}	3.11×10^{-5}	3.22×10^{-5}	3.06×10^{-5}	0.0068
e_r	2.42%	2.96%	0.65%	0.09%	0.30%	

Randomly generate $K=100$ test points to evaluate the Kriging models constructed using different sampling methods. The mean absolute relative error (MARE) is used as the criterion to measure the accuracy of the surrogate model, which is defined as:

$$\text{MARE}=\frac{1}{K}\sum_{i=1}^{K}\left|\frac{y_i-\hat{y}_i}{y_i}\right|, \tag{4.2}$$

where $\hat{y}_i$ denotes t the predicted response calculated by the surrogate model, and y_i denotes the actual response of the machine tool. It can be seen from Table 6 that the five-point response errors of the DES-Kriging model of the machine tool are all within 5%, and the computational efficiency of the DES-Kriging model is more than 6000 times that of the finite element model. It can be seen from Table 7 that for each point, the MARE of the DES-Kriging model is smaller than that of the traditional Kriging model, and the MARE of the DES-Kriging model is within 5%. This shows that different point-set construction methods and sample sizes have a significant impact on the accuracy of the Kriging surrogate model. Adopting the DES point set as the initial sampling data for Kriging modeling enhances the surrogate model's predictive precision.

Table 7. Two models are used to solve the MARE of 100 test sets.

	MARE				
Model	1	2	3	4	5
Kriging model	6.75%	7.08%	2.32%	1.77%	2.04%
DES-Kriging model	4.32%	4.78%	2.04%	1.56%	1.22%

4.3. Interval analysis of machine tools using DAK method

In Sections 4.1 and 4.2, we propose the DES-ABC algorithm and establish the DES-Kriging model of the machine tool beam response. Next, we apply DAK to interval analysis of machine tools. The spring stiffness and the force position are used as interval variables, the DES-Kriging model of the beam is used to solve the response of the dangerous point, and the ABC algorithm is used to find the range of the response value. The Monte Carlo simulation method (the number of samples set to 10^5 and 10^6, respectively) and DAK are used for uncertainty analysis. When employing the DAK method for analysis, the calculation is terminated when the range of the obtained response values surpasses that derived from the Monte Carlo method with a sample size of 10^6. The computational outcomes and the number of computations is then recorded. This process is conducted 10 times to

determine the mean and variance of both the computational results and the number of computations. The specific ranges and variances of the five-point responses can be observed in the following Table 8.

Table 8. Comparison of Monte Carlo method and this method.

Selected points range		Monte Carlo simulation method		Method of this article		Standard deviation	
		10^5	10^6	result	number of total calculations	s_{res} (Unit: 10^{-4})	s_{cal}
Test point 1	lower bound	2.622×10^{-5}	2.590×10^{-5}	2.581×10^{-5}	1918	6.074×10^{-8}	528
	upper bound	3.498×10^{-5}	3.554×10^{-5}	3.558×10^{-5}	1774	4.141×10^{-8}	272
Test point 2	lower bound	2.625×10^{-5}	2.620×10^{-5}	2.607×10^{-5}	1198	8.087×10^{-8}	226
	upper bound	3.437×10^{-5}	3.500×10^{-5}	3.521×10^{-5}	2446	17.69×10^{-8}	699
Test point 3	lower bound	2.975×10^{-5}	2.966×10^{-5}	2.960×10^{-5}	2290	4.499×10^{-8}	419
	upper bound	3.275×10^{-5}	3.290×10^{-5}	3.295×10^{-5}	2416	4.199×10^{-8}	807
Test point 4	lower bound	3.142×10^{-5}	3.121×10^{-5}	3.119×10^{-5}	3094	1.959×10^{-8}	549
	upper bound	3.345×10^{-5}	3.387×10^{-5}	3.397×10^{-5}	2596	6.582×10^{-8}	704
Test point 5	lower bound	2.971×10^{-5}	2.949×10^{-5}	2.948×10^{-5}	2932	9.342×10^{-7}	597
	upper bound	3.299×10^{-5}	3.323×10^{-5}	3.330×10^{-5}	1294	4.943×10^{-8}	282

As shown in Table 8, when employing DAK for interval uncertainty analysis of the machine tool beam model, a minimum of only 1198 simulations is required to obtain a more conservative lower bound compared to the Monte Carlo method at the same computational scale. Even in the most demanding case, only 3094 simulations are needed to determine a less conservative upper bound that exceeds the Monte Carlo results. The DAK method proposed in this paper is used to analyze the interval uncertainty, and a larger response boundary than the Monte Carlo method can be obtained by calculating 21,958 responses. Compared with the Monte Carlo method, the efficiency of the DES-ABC method is improved by three orders of magnitude, and the calculation accuracy is higher than that of the Monte Carlo method. Therefore, it can be considered that the method proposed in this paper can accurately and efficiently analyze the interval uncertainty of the machine tool beams. The standard deviations of the calculation results and the number of calculations show the average degree of deviation of data points from the mean, indicating that the DAK method has strong algorithmic stability.

In summary, we have proposed an efficient and accurate interval uncertainty analysis method for machine tools, which can perform uncertainty analysis on the responses of key positions of machine tools and obtain the specific range of responses, providing important support for machine tool design, machining accuracy improvement, and stability assurance.

5. Conclusions

The stiffness of the beam joint of the machine tool is affected by many uncertain factors during use, which may lead to changes in the performance of the machine tool. It is necessary to perform interval uncertainty analysis on the machine tool to ensure its smooth operation.

Aiming at the uncertainty of beam stiffness of the gantry machine tool, an improved interval

analysis method based on the DES-ABC and DES-Kriging model is proposed in this paper. The DES point set optimization ABC algorithm is used to solve the problem of low search efficiency caused by the uneven distribution of random sequences in the traditional ABC algorithm. Experiments show that the DES-ABC algorithm is significantly better than the original algorithm in terms of convergence accuracy and speed. The computational accuracy of the DES-ABC algorithm has been improved by 80% compared to the ABC algorithm, and its computational efficiency is about 3.5 times higher than the traditional ABC algorithm. By constructing the Kriging model of the machine tool beam, the computational burden of the finite element model is effectively reduced. The single calculation efficiency of the Kriging model is more than 6,000 times that of the finite element model. At the same time, the DES sequence is used to replace the original sample of the Kriging model, which makes the original sample of the Kriging model more uniform. Experiments show that the introduction of the DES sequence improves the accuracy of the Kriging model, keeping the error of the calculation results within 5%, and the DES-Kriging model can accurately solve the machine tool response. In the interval analysis of the machine tool beams, the proposed method accurately obtains the displacement response boundary of key points with very low computational cost, which is three orders of magnitude more efficient than the Monte Carlo method. By integrating the DES-Kriging model with the DES-ABC algorithm, this paper successfully proposes an efficient and accurate uncertainty analysis method for machine tools, known as the DAK method. In general, the method proposed in this paper not only improves the accuracy and efficiency of machine tool interval analysis but also provides important support for machine tool design, machining accuracy improvement, and stability assurance. The proposed combination method of DES-ABC and DES-Kriging can be widely used in the optimization design and uncertainty analysis of complex engineering structures and has high practical value and promotion potential.

Author contributions

Xindi Wei: conceptualization, methodology, software, validation, writing-original draft and editing; Jin Deng: conceptualization, methodology, project administration, supervision, funding acquisition, writing-review and editing; Shizhong Liang: conceptualization, writing-review and editing, resources; Yu Ye: methodology, software, investigation. All authors have read and approved the final version of the manuscript for publication. Xindi Wei and Jin Deng contributed equally to this work and are co-first authors.

Use of Generative-AI tools declaration

The authors declare that they have not used Artificial Intelligence (AI) tools in the creation of this article.

Acknowledgments

This work was supported by the “Yunnan Provincial Key R&D Program” Yunnan International Joint R&D Center for Engineering Simulation and Analysis of High-end Equipment (No. 202403AP140034).

Conflict of interest

The authors declare no conflicts of interest.

References

1. S. J. Guo, G. D. Jiang, X. S. Mei, Investigation of sensitivity analysis and compensation parameter optimization of geometric error for five-axis machine tool, *Int. J. Adv. Manuf. Technol.*, **93** (2017), 3229–3243. https://doi.org/10.1007/s00170-017-0755-6
2. Q. Cheng, W. D. Ren, Z. F. Liu, D. J. Chen, P. H. Gu, Load-induced error identification of hydrostatic turntable and its influence on machining accuracy, *J. Cent. South Univ.*, **23** (2016), 2558–2569. https://doi.org/10.1007/s11771-016-3317-4
3. D. Zhang, L. H. Wang, Z. Gao, X. P. Su, On performance enhancement of parallel kinematic machine, *J. Intell. Manuf.*, **24** (2013), 267–276. https://doi.org/10.1007/s10845-011-0583-8
4. H. L. Fang, T. F. Tang, Z. He, Y. C. Liu, J. Zhang, A novel hybrid machine tool integrating a symmetrical redundantly actuated parallel mechanism: design, kinematics, prototype and experiment, *Mech. Mach. Theory.*, **176** (2022), 105013. https://doi.org/10.1016/j.mechmachtheory.2022.105013
5. L. Li, Q. Q. Yun, Z. Q. Li, Y. Liu, C. Y. Cao, A new contact model of joint surfaces accounting for surface waviness and substrate deformation, *Int. J. Appl. Mech.*, **11** (2019), 1950079. https://doi.org/10.1142/S1758825119500790
6. M. Burdekin, N. Back, A. Cowley, Analysis of the local deformations in machine joints, *Journal of Mechanical Engineering Scienc*e, **21** (1979), 25–32.
7. F. Wu, D. W. Huang, X. M. Xu, K. Zhao, N. Zhou, An adaptive divided-difference perturbation method for solving stochastic problems, *Struct. Saf.*, **103** (2023), 102346. https://doi.org/10.1016/j.strusafe.2023.102346
8. F. Wu, W. X. Zhong, A hybrid approach for the time domain analysis of linear stochastic structures, *Comput. Method. Appl. M.*, **265** (2013), 71–82. https://doi.org/10.1016/j.cma.2013.06.006
9. D. W. Huang, F. Wu, S. Zhang, B. S. Chen, H. W. Zhang, A high-performance calculation scheme for stochastic dynamic problems, *Mech. Syst. Signal Pr.*, **189** (2023), 110073. https://doi.org/10.1016/j.ymssp.2022.110073
10. D. W. Huang, F. Wu, Y. L. Zhao, J. Yan, H. W. Zhang, Application of high-credible statistical results calculation scheme based on least squares Quasi-Monte Carlo method in multimodal stochastic problems, *Comput. Method. Appl. M.*, **418** (2024), 116576. https://doi.org/10.1016/j.cma.2023.116576
11. X.-X. Liu, Q.-Z. Xie, R.-J. Du, F. Zhang, Real-world engineering problems: Two surrogate methods for robust vibration control of moving mass-beam coupling systems with epistemic uncertainty, *Aerosp. Sci. Technol.*, **130** (2022), 107916. https://doi.org/10.1016/j.ast.2022.107916
12. M. A. Hariri-Ardebili, B. Sudret, Polynomial chaos expansion for uncertainty quantification of dam engineering problems, *Eng. Struct.*, **203** (2020), 109631. https://doi.org/10.1016/j.engstruct.2019.109631
13. D. Yuan, Q. Wan, D. Wang, Influence of bolt preload degradation on nonlinear vibration responses of jointed structures, *J. Sound Vib.*, **595** (2025), 118797. https://doi.org/10.1016/j.jsv.2024.118797

14. W. J. Pan, X. P. Li, L. L. Wang, N. Guo, Z. M. Yang, Influence of contact stiffness of joint surfaces on oscillation system based on the fractal theory, *Arch. Appl. Mech.*, **88** (2018), 525–541. https://doi.org/10.1007/s00419-017-1325-y
15. Z. X. Wang, Y. Q. Wang, G. X. Zhang, Y. J. Shi, Tests and parametric analysis of aluminum alloy bolted joints of different material types, *Constr. Build. Mater.*, **185** (2018), 589–599. https://doi.org/10.1016/j.conbuildmat.2018.07.062
16. R. B. Patil, M. A. Mellal, A. K. Bewoor, S. Al-Dahidi, Reliability, maintainability, and availability analysis of a computerized numerical control machine tool using Markov chains, *Acta Polytech. Hung.*, **18** (2021), 45–70. https://doi.org/10.12700/APH.18.6.2021.6.3
17. X. Du, J. L. Huo, L. Chen, M. C. Wang, Z. S. Wu, C. L. Zhang, Application of intelligent optimization algorithms in the distribution network planning and evaluation models, *Procedia Computer Science*, **228** (2023), 1205–1214. https://doi.org/10.1016/j.procs.2023.11.106
18. F. Wu, L. Zhu, Y. L. Zhao, C. F. Ai, X. Wang, F. Cai, et al., Wave spectrum fitting with multiple parameters based on optimization algorithms and its application, *Ocean Eng.*, **312** (2024), 119073. https://doi.org/10.1016/j.oceaneng.2024.119073
19. D. Karaboga, An idea based on honey bee swarm for numerical optimization, *Technical Report-Tr06*, Erciyes University, (2005), http://mf.erciyes.edu.tr/abc/pub/tr06_2005.pdf
20. H. B. Zhao, M. Zhao, C. X. Zhu, Reliability-based optimization of geotechnical engineering using the artificial bee colony algorithm, *KSCE J. Civ. Eng.*, **20** (2016), 1728–1736. https://doi.org/10.1007/s12205-015-0117-6
21. S. N. Shivappriya, T. Gowrishankar, G. Stoian, J. Anitha, D. J. Hemanth, Enhancing performance of parallel hybrid electric vehicles using Powell's artificial bee colony method, *Heliyon*, **11** (2025), e42325. https://doi.org/10.1016/j.heliyon.2025.e42325
22. Y. B. Cui, W. Hu, A. Rahmani, Fractional-order artificial bee colony algorithm with application in robot path planning, *Eur. J. Oper. Res.*, **306** (2023), 47–64. https://doi.org/10.1016/j.ejor.2022.11.007
23. Y. L. Zhao, F. Wu, J. H. Pang, W. X. Zhong, New heterogeneous comprehensive learning particle swarm optimizer enhanced with low-discrepancy sequences and conjugate gradient method, *Swarm Evol. Comput.*, **93** (2025) 101848. https://doi.org/10.1016/j.swevo.2025.101848
24. F. De Rainville, C. Gagné, O. Teytaud, D. Laurendeau, Evolutionary optimization of low-discrepancy sequences, *ACM T. Model. Comput. S.*, **22** (2012), 1–25. https://doi.org/10.1145/2133390.2133393
25. F. Wu, Y. L. Zhao, K. Zhao, W. X. Zhong, A multi-body dynamical evolution model for generating the point set with best uniformity, *Swarm Evol. Comput.*, **73** (2022), 101121. https://doi.org/10.1016/j.swevo.2022.101121
26. F. Wu, W. X. Zhong, A modified stochastic perturbation method for stochastic hyperbolic heat conduction problems, *Comput. Method. Appl. M.*, **305** (2016), 739–758, https://doi.org/10.1016/j.cma.2016.03.032
27. F. Wu, W. X. Zhong, On displacement shallow water wave equation and symplectic solution, *Comput. Method. Appl. M.*, **318** (2017), 431–455. https://doi.org/10.1016/j.cma.2017.01.040
28. F. A. C. Viana, C. Gogu, T. Goel, Surrogate modeling: tricks that endured the test of time and some recent developments, *Struct. Multidisc. Optim.*, **64** (2021), 2881–2908. https://doi.org/10.1007/s00158-021-03001-2

29. C. L. He, Y. Zhang, D. W. Gong, X. F. Ji, A review of surrogate-assisted evolutionary algorithms for expensive optimization problems, *Expert Syst. Appl.*, **217** (2023), 119495. https://doi.org/10.1016/j.eswa.2022.119495
30. Z. Azarhoosh, M. I. Ghazaan, A review of recent advances in surrogate models for uncertainty quantification of high-dimensional engineering applications, *Comput. Method. Appl. M.*, **433** (2025), 117508. https://doi.org/10.1016/j.cma.2024.117508
31. X. H. Peng, J. Q. Kou, W. W. Zhang, Multi-fidelity nonlinear unsteady aerodynamic modeling and uncertainty estimation based on Hierarchical Kriging, *Appl. Math. Model.*, **122** (2023), 1–21. https://doi.org/10.1016/j.apm.2023.05.031
32. A. Thapa, A. Roy, S. Chakraborty, Reliability analysis of underground tunnel by a novel adaptive Kriging based metamodeling approach, *Probabilist. Eng. Mech.*, **70** (2022), 103351. https://doi.org/10.1016/j.probengmech.2022.103351
33. J. Kudela, R. Matousek, Recent advances and applications of surrogate models for finite element method computations: a review, *Soft Comput.*, **26** (2022), 13709–13733. https://doi.org/10.1007/s00500-022-07362-8
34. Z. P. Qiu, C. Y. Ju, A comparative study of probabilistic and Non-probabilistic models for the stress intensity factors of embedded cracks, *Eng. Fract. Mech.*, **259** (2022), 108105. https://doi.org/10.1016/j.engfracmech.2021.108105
35. C. Jiang, X. Han, G. Y. Lu, J. Liu, Z. Zhang, Y. C. Bai, Correlation analysis of non-probabilistic convex model and corresponding structural reliability technique, *Comput. Method. Appl. M.*, **200** (2011), 2528–2546. https://doi.org/10.1016/j.cma.2011.04.007
36. B. Y. Ni, C. Jiang, Z. L. Huang, Discussions on non-probabilistic convex modelling for uncertain problems, *Appl. Math. Model.*, **59** (2018), 54–85. https://doi.org/10.1016/j.apm.2018.01.026
37. D. Karaboga, B. Basturk, A powerful and efficient algorithm for numerical function optimization: artificial bee colony (ABC) algorithm, *J. Glob. Optim.*, **39** (2007), 459–471. https://doi.org/10.1007/s10898-007-9149-x
38. E. B. Andres, Kriging, In: *Encyclopedia of environmetrics*, 2 Eds., New York: John Wiley & Sons, Ltd., 2013. https://doi.org/10.1002/9780470057339.vak003.pub2
39. G. Pistone, G. Vicario, Comparing and generating Latin Hypercube designs in Kriging models, *AStA Adv. Stat. Anal.*, **94** ((2010), 353–366. https://doi.org/10.1007/s10182-010-0142-1
40. F. Wu, K. Zhao, X. L. Wu, H. J. Peng, L. L. Zhao, W. X. Zhong, A time-averaged method to analyze slender rods moving in tubes, *Int. J. Mech. Sci.*, **279** (2024), 109510. https://doi.org/10.1016/j.ijmecsci.2024.109510
41. F. Wu, Y. L. Zhao, Y. X. Yang, X. P. Zhang, N. Zhou, A new discrepancy for sample generation in stochastic response analyses of aerospace problems with uncertain parameters, *Chinese J. Aeronaut.*, **37** (2024), 192–211. https://doi.org/10.1016/j.cja.2024.09.044
42. O. Teytaud, S. Gelly, DCMA, yet another derandomization in covariance-matrix-adaptation, In: *Proceedings of the 9th annual conference on Genetic and evolutionary computation*, New York: Association for Computing Machinery, 2007, 955–963. https://doi.org/10.1145/1276958.1277150
43. S. S. Garud, I. A. Karimi, M. Kraft, Design of computer experiments: a review, *Comput. Chem. Eng.*, **106** (2017), 71–95. https://doi.org/10.1016/j.compchemeng.2017.05.010
44. G. Ökten, Y. N. Liu, Randomized quasi-Monte Carlo methods in global sensitivity analysis, *Reliab. Eng. Syst. Safe.*, **210** (2021), 107520. https://doi.org/10.1016/j.ress.2021.107520

45. Karishma, H. Kumar, A new hybrid particle swarm optimizationalgorithm for optimal tasks scheduling in distributed computing system, *Intelligent Systems with Applications*, **18** (2023), 200219. https://doi.org/10.1016/j.iswa.2023.200219
46. B. Sun, W, Li, Y. Huang, Performance of composite PPSO on single objective bound constrained numerical optimization problems of CEC 2022, *2022 IEEE Congress on Evolutionary Computation*, Padua, Italy, 2022, 1–8. https://doi.org/10.1109/CEC55065.2022.9870369
47. C. Li, X. D. Wei, C. Y. Chen, J. H. Tang, Adaptive time-stepping approach for efficient interval uncertainty analysis of control rod drop dynamics, *J. Nonlinear Math. Phys.*, **32** (2025), 42. https://doi.org/10.1007/s44198-025-00294-5

Appendix A. The specific forms of benchmark test functions

The specific forms of benchmark test functions are shown in this appendix. The benchmark test function is composed of 16 basic functions as follows:

1) Rosenbrock's Function

$$f_1(\boldsymbol{x}) = \sum_{i=1}^{D-1}\left[100\left(x_{i+1} - x_i^2\right)^2 + \left(x_i - 1\right)^2\right]. \tag{A.1}$$

2) Expanded Schaffer's Function

$$\begin{aligned} g(y,z) &= 0.5 + \frac{\sin^2\left(\sqrt{y^2+z^2}\right) - 0.5}{\left(1 + 0.001(y^2+z^2)\right)^2} \\ f_2(\boldsymbol{x}) &= g(x_1,x_2) + g(x_2,x_3) + \cdots + g(x_{D-1},x_D) + g(x_D,x_1) \end{aligned}. \tag{A.2}$$

3) Rastrigin's Function

$$f_3(\boldsymbol{x}) = \sum_{i=1}^{D}\left(x_i^2 - 10\cos(2\pi x_i) + 10\right). \tag{A.3}$$

4) Levy Function

$$\begin{aligned} &f_4(\boldsymbol{x}) = \sin^2(\pi w_1) + \sum_{i=1}^{D-1}\left[\left(w_i - 1\right)^2\left(1 + 10\sin^2(\pi w_i + 1)\right)\right] + \left(w_D - 1\right)^2\left(1 + \sin^2(2\pi w_D)\right) \\ &\text{where } w_i = 1 + \frac{x_i - 1}{4},\ \forall i = 1,\ldots,D \end{aligned} \tag{A.4}$$

5) Bent Cigar Function

$$f_5(\boldsymbol{x}) = x_1^D + 10^{6\sum_{i=2}^{D} x_i^2}. \tag{A.5}$$

6) HGBat Function

$$f_6(\boldsymbol{x}) = \left| \left(\sum_{i=1}^{D} x_i^2 \right)^2 - \left(\sum_{i=1}^{D} x_i \right)^2 \right|^{0.5} + \frac{0.5\sum_{i=1}^{D} x_i^2 + \sum_{i=1}^{D} x_i}{D} + 0.5. \tag{A.6}$$

7) High Conditioned Elliptic Function

$$f_7(\boldsymbol{x}) = \sum_{i=1}^{D} \left(10^6\right)^{\frac{i-1}{D-1}} x_i^2. \tag{A.7}$$

8) Katsuura Function

$$f_8(\boldsymbol{x}) = \frac{10}{D^2} \prod_{i=1}^{D} \left(1 + i \sum_{j=1}^{32} \frac{\left| 2^j x_i - \text{round}\left(2^j x_i\right) \right|}{2^j} \right)^{\frac{10}{2^j}} - \frac{10}{D^2}. \tag{A.8}$$

9) Happycat Function

$$f_9(\boldsymbol{x}) = \left| \sum_{i=1}^{D} x_i^2 - 1 \right|^{0.25} + \frac{0.5\sum_{i=1}^{D} x_i^2 + \sum_{i=1}^{D} x_i}{D} + 0.5. \tag{A.9}$$

10) Expanded Rosenbrock's plus Griewangk's Function

$$f_{10}(\boldsymbol{x}) = f_{14}\left(f_1(x_1, x_2)\right) + f_{14}\left(f_1(x_2, x_3)\right) + \cdots f_{14}\left(f_1(x_{D-1}, x_D)\right) + f_{14}\left(f_1(x_D, x_1)\right). \tag{A.10}$$

11) Modified Schwefel's Function

$$\begin{aligned} f_{11}(\boldsymbol{x}) &= 418.9829 \times D - \sum_{i=1}^{D} g(x_i) \\ z_i &= x_i + 4.209687464475036 \times 10^2 \\ g(z_i) &= \begin{cases} z_i \sin\left(\sqrt{|z_i|}\right) & |z_i| \le 500 \\ \left(500 - \text{mod}\left(z_i, 500\right)\right) \sin\left(\sqrt{500 - \text{mod}(z_i, 500)}\right) - \dfrac{\left(z_i - 500\right)^2}{100000} & z_i > 500 \\ \left(\text{mod}\left(|z_i|, 500\right) - 500\right) \sin\left(\sqrt{|\text{mod}(|z_i|, 500) - 500|}\right) - \dfrac{z_i^2}{100000} & z_i < -500 \end{cases} \end{aligned} \tag{A.11}$$

12) Ackley's Function

$$f_{12}(\boldsymbol{x}) = -20\exp\left(-0.2\sqrt{\frac{1}{D}\sum_{i=1}^{D} x_i^2} \right) - \exp\left(\frac{1}{D}\sum_{i=1}^{D} \cos(2\pi x_i) \right) + 20 + e. \tag{A.12}$$

13) Discus Function

$$f_{13}(\boldsymbol{x}) = 10^{10} x_1^2 + \sum_{i=2}^{D} x_i^2 \ . \tag{A.13}$$

14) Griewank's Function

$$f_{14}(\boldsymbol{x}) = \sum_{i=1}^{D} \frac{x_i^2}{4000} - \prod_{i=1}^{D} \cos\left(\frac{x_i}{\sqrt{i}}\right) + 1. \tag{A.14}$$

15) Schaffer's F7 Function

$$f_{15}(\boldsymbol{x}) = \left(\frac{1}{D-1}\sum_{i=1}^{D-1}\left(\sqrt{s_i}\right)\sin^2\left(50\left(s_i\right)^{0.2}+1\right)\right)^2, \ \ s_i = \sqrt{x_i^2 + x_{i+1}^2} \ . \tag{A.15}$$

The first benchmark test function F1 is Shifted and full Rotated Expanded Schaffer's F7, which is shown as,

$$F_1(\boldsymbol{x}) = f_2\left(\boldsymbol{M}\frac{0.5(\boldsymbol{x}-\boldsymbol{o})}{100}\right) + F_1^*, \tag{A.16}$$

where $\boldsymbol{M}$ is the rotation matrix, $\boldsymbol{o}$ is the shifted global optimum, and $F_1^* = 600$ is shown in Table 1. Besides, The second benchmark test function F2 is the Shifted and Rotated Levy Function as follows,

$$F_2(\boldsymbol{x}) = f_4\left(\boldsymbol{M}\left(\frac{5.12(\boldsymbol{x}-\boldsymbol{o})}{100}\right)\right) + F_2^*, \tag{A.17}$$

where $F_2^* = 900$ is shown in Table 1. And the third and fourth benchmark test functions are both hybrid functions. In the hybrid functions, the variables are randomly divided into some subcomponents and then different basic functions are used for different subcomponents.

$$F(\boldsymbol{x}) = g_1(\boldsymbol{M}_1 \boldsymbol{z}_1) + g_2(\boldsymbol{M}_2 \boldsymbol{z}_2) + \cdots + g_n(\boldsymbol{M}_n \boldsymbol{z}_n) + F^*, \tag{A.18}$$

where $F(\boldsymbol{x})$ is the hybrid function, $g_i(\bullet)$ is the i-th basic function, n is the number of basic function, and $\boldsymbol{z}_i$ is shown as follows:

$$\begin{cases} z_1 = \left[x_1 - o_1, x_2 - o_2, \cdots x_{D_1} - o_{D_1} \right] \\ z_2 = \left[x_{D_1+1} - o_{D_1+1}, x_{D_1+2} - o_{D_1+2}, \cdots x_{D_1+D_2} - o_{D_1+D_2} \right] \\ \cdots \\ z_n = \left[x_{\sum_{i=1}^{n-1} D_i+1} - o_{\sum_{i=1}^{n-1} D_i+1}, x_{\sum_{i=1}^{n-1} D_i+2} - o_{\sum_{i=1}^{n-1} D_i+2}, \cdots x_D - o_D \right] \\ D_i = \begin{cases} \lceil p_i D \rceil, & i = 1,2,\cdots,n-1 \\ D - \sum_{j=1}^{n-1} D_j \end{cases} \end{cases} \tag{A.19}$$

The parameters of the third benchmark test function F3 are as follows, $n = 6$, $\boldsymbol{p} = [0.1, 0.2, 0.2, 0.2, 0.2, 0.1, 0.2]$, $g_i(\bullet)$ is HGBat Function f_6, Katsuura Function f_8, Ackley's Function f_{12}, Rastrigin's Function f_3, Modified Schwefel's Function f_{11}, and Schaffer's F7 Function f_{15}, respectively. And the parameters of the forth benchmark test function F4 are as follows, $n = 5$, $\boldsymbol{p} = [0.3, 0.2, 0.2, 0.1, 0.2]$, $g_i(\bullet)$ is HGBat Function f_6, HappyCat Function f_9, Expanded Griewank's plus Rosenbrock's Function f_{10}, Modified Schwefel's Function f_{11}, and Ackley's Function f_{12}, respectively. In addition, the last benchmark test function F5 is the composition function,

$$F(\boldsymbol{x}) = \sum_{i=1}^{5} \left\{ \omega_i \left[\lambda_i g_i(\boldsymbol{x}) + \text{bias}_i \right] \right\} + F_5^*, \tag{A.20}$$

where $g_i(\bullet)$, $i = 1,2,\cdots,5$, is Rotated Rosenbrock's Function f_1, High Conditioned Elliptic Function f_7, Rotated Bent Cigar Function f_5, Rotated Discus Function f_{13} and High Conditioned Elliptic Function f_7. $\lambda = \left[1, 1\times10^{-6}, 1\times10^{-6}, 1\times10^{-6}\right]$, bias$=[0, 200, 300, 100, 400]$, $\omega_i = w_i / \sum_{i=1}^{n} w_i$, $w_i = \dfrac{1}{\sqrt{\sum_{i=1}^{D} \left(x_j - o_{ij}\right)^2}} \exp\left(-\dfrac{\sum_{j=1}^{D} \left(x_j - o_{ij}\right)^2}{2D\sigma_i^2} \right)$, $\sigma = [10, 20, 30, 40, 50]$.